Histidine-Derived Nontoxic Nitrogen-Doped Carbon Dots for Sensing and Bioimaging Applications

ARTICLE *in* LANGMUIR · NOVEMBER 2014

Impact Factor: 4.46 · DOI: 10.1021/la503969z · Source: PubMed

9 AUTHORS, INCLUDING:

Shoujun Zhu
Stanford University
47 PUBLICATIONS **1,824** CITATIONS
SEE PROFILE

Hailong Wang
Jilin University
17 PUBLICATIONS **36** CITATIONS
SEE PROFILE

Langmuir

Article

pubs.acs.org/Langmuir

Histidine-Derived Nontoxic Nitrogen-Doped Carbon Dots for Sensing and Bioimaging Applications

He Huang,[†] Chunguang Li,*[,†] Shoujun Zhu,[‡] Hailong Wang,[‡] Cailing Chen,[†] Zhaorui Wang,[†] Tianyu Bai,[†] Zhan Shi,*[,†] and Shouhua Feng[†]

[†]State Key Laboratory of Inorganic Synthesis and Preparative Chemistry, College of Chemistry, and [‡]State Key Laboratory of Supramolecular Structure and Materials, College of Chemistry, Jilin University, Changchun, Jilin 130012, People's Republic of China

Supporting Information

ABSTRACT: Nitrogen-doped (N-doped) photoluminescent carbon dots (CDs) were prepared by a one-pot microwave-assisted hydrothermal treatment using histidine as the sole carbon source in the absence of acid, alkali, or metal ions. With a diameter of 2−5 nm, the synthesized CDs had apparent lattice fringes and exhibited an excitation-dependent photoluminescent behavior. The CDs were highly yielded, well-dispersed in aqueous solution, and showed high photostability in the solutions of a wide range of pH and salinity. They were used as probes to identify the presence of Fe^{3+} ions with a detection limit of 10 nM. With confirmed nontoxicity, these CDs could enter the cancer cells, indicating a practical potential for cellular imaging and labeling.

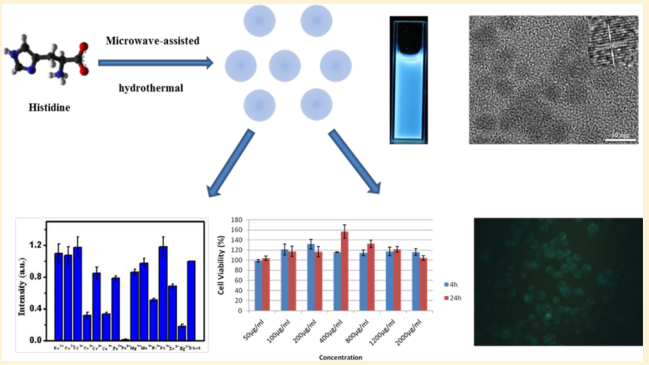

1. INTRODUCTION

Fluorescent nanomaterials have drawn increasing attention because of their optical properties and diverse applications, such as energy-saving display, lighting, optoelectric devices, and biology markers.[1−3] To date, traditional photoluminescent (PL) materials containing lead, cadmium, gold, silver, and silicon have been extensively synthesized.[4−7] These materials, however, have raised concerns over potential toxicity, environmental hazard, and cost-effectiveness.[7,8] Therefore, it is of great importance to develop simple, environmentally friendly, and low-cost methods for the synthesis of fluorescent nanomaterials with superior photoluminescence and minimal toxicity.

In recent years, carbon dots (CDs), which are small carbon nanoparticles less than 10 nm in size, have attracted broad attention from both academia and industry because of their outstanding advantages, such as stable PL properties, robust chemical inertness, high aqueous solubility, biocompatibility, versatile surface chemistry, and low toxicity.[9−12] The preparative approaches of CDs can be divided into two major categories, i.e., top-down and bottom-up strategies. The top-down strategies include laser ablation,[13−15] arc discharge,[16] and electrochemical oxidation,[17,18] where CDs are derived from graphite and its derivatives. The bottom-up strategies are normally adopted to prepare CDs by carbonization of carbonaceous organic matter using methods, such as solvothermal methods,[19−21] pyrolysis,[22] microwave treatment,[23] supported methods,[24] and ultrasonic-assisted synthetic methods.[25] Among these strategies, microwave methods have distinct advantages, such as being fast, simple, and high-powered. Recently, molecular carbon precursors, such as carbohydrate,[26] polyhydric alcohol,[27] and polyhydric acid,[28] were employed to synthesize CDs. Biological precursors, such as soybean milk,[29] pomelo peel,[30] and strawberry juice,[31] were also used to prepare CDs as green methods. However, to produce CDs with adequate quantum yields (QYs) of fluorescence, a surface-passivating procedure is necessary.[13] Otherwise, highly PL CDs could be synthesized using nitrogen-containing precursors without surface-passivating agents.[21,28] Histidine is a nitrogen-rich essential amino acid in humans and other mammals with an imidazole functional group. Cui et al. have prepared CDs using amino acid as a precursor under acid or alkali conditions through a microwave pyrolysis process.[32] However, the presence of acids or alkali may be detrimental to the biocompatibility of the resulting CDs and their performance in bioimaging application.

Herein, we report on a one-pot microwave-assisted hydrothermal approach to prepare fluorescent nitrogen-doped carbon dots (N-CDs) derived from histidine. In comparison to previous work using histidine to prepare N-CDs, our method does not need any additives (acid, alkali, or salt), organic solvent, or further surface modification/passivation. The synthesis was conducted at mild reaction conditions. The as-synthesized N-CDs with defined surface chemistry and properties could be well-dispersed in an aqueous solution and display an excitation tunable luminescence as well as high photostability in different pH values and different concen-

Received: October 6, 2014
Revised: October 25, 2014
Published: November 6, 2014

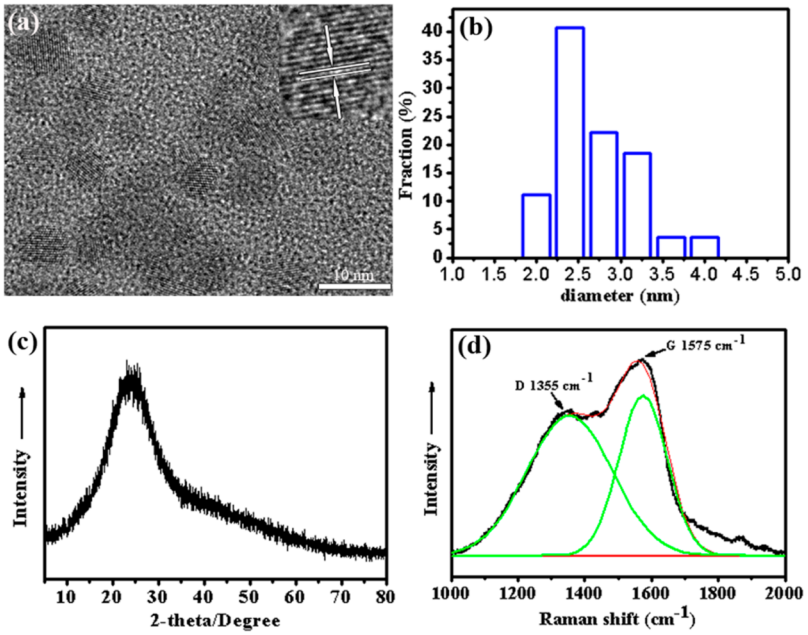

Figure 1. (a) TEM image of C-60, with the scale bar of 10 nm, (inset) corresponding HRTEM image of C-60, (b) particle size distribution histograms of C-60, (c) XRD pattern of C-60, and (d) Raman spectrum of C-60.

trations of KCl aqueous solutions. In addition, a nearly null toxicity and favorable biocompatibility associated with the as-prepared N-CDs qualified them as a probe to detect different metal ions, making them a promising candidate for cellular imaging.

2. EXPERIMENTAL SECTION

2.1. Chemicals and Materials. Hisitidine, $FeCl_3$, $FeCl_2$, $CrCl_3$, $Cu(NO_3)_2$, $NiCl_2$, $CoCl_2$, $Mg(CH_3COO)_2$, $ZnCl_2$, $CdCl_2$, $MnCl_2$, $Hg(NO_3)_2$, $PbCl_2$, $BaCl_2$, $CaCl_2$, KCl, and NaOH were purchased from Sinopharm Chemical Reagent Co., Ltd, China. The dialysis bag was purchased from Shanghai Yuanye Bio-Technology Co., Ltd., China.

2.2. Synthesis of CDs. A commercial microwave reactor (Ethos One, Italy) system was used to prepare the N-CDs. A total of 1.1647 g of histidine was dissolved in 30 mL of deionized (DI) water. The mixture was ultrasonicated for 10 min to yield a clear solution. Then, the solution was added to the reaction vessel of the microwave reactor. A total of 4 min was required to elevate the temperature of the reaction vessel up to 200 °C. The reaction vessel was maintained at 200 °C for 10, 30, and 60 min by microwave irradiation and then cooled to room temperature. The product, a brownish black and transparent aqueous solution, was subjected to dialysis (M_w = 1000) for 2 days to eliminate the overreacted residue.

2.3. Metal Ion Detection. Many metal ion sources have been used to detect metal ions, such as $FeCl_3$, $FeCl_2$, $CrCl_3$, $Cu(NO_3)_2$, $NiCl_2$, $CoCl_2$, $Mg(CH_3COO)_2$, $ZnCl_2$, $CdCl_2$, $MnCl_2$, $Hg(NO_3)_2$, $PbCl_2$, $BaCl_2$, and $CaCl_2$. In this study, all chemicals were used without further purification. N-CD solution (0.01 mg/mL) was used to detect the metal ion (a calculated amount of ions of 10^{-3} M). The spectra were recorded after reaction for 3 min. The excited wavelength was set at 360 nm for all of the PL spectra.

2.4. Characterization. Microstructural images of the CDs were recorded on high-resolution transmission electron microscopy (HTEM), Tecnai G2 S-Twin F20 [the decreased electrobeam intensity and increased exposure time can be beneficial to the obtained transmission electron microscopy (TEM) images of N-CDs]. Fluorescence spectroscopy was carried out using a FLUOROMAX-4 spectrophotometer (JY company). Ultraviolet−visible (UV−vis) absorption spectra were measured with a Shimadzu UV-2450 UV−vis spectrophotometer. Fourier transform infrared spectroscopy (FTIR) was performed with on a Nicolet AVATAR 360 FTIR spectrophotometer. The fluorescent images were captured with Olympus BX51 at UV light excitations. The color filters were integrated in the fluorescence microscope, with no extra filters needed. Raman spectra were measured with a JY-T64000 Raman spectrometer (HORIBA Jobin Yvon) with radiation at 514 nm. X-ray photoelectron spectroscopy (XPS) was conducted on an ESCALAB 250 spectrometer with a mono X-ray source with Al Kα excitation (1486.6 eV). Binding energy calibration was based on C 1s at 284.7 eV. X-ray diffraction (XRD) was investigated by a Rigaku D/Max 2500 diffractometer with a graphite monochromator using Cu Kα radiation operating at 200 mA and 40 kV. Fluorescence decay spectra were performed with a FLS980 (Edinburgh Instruments).

2.5. QY Measurements. The QYs of the resultant N-CDs were measured by the following equation:

$$Q = Q_R I/I_R \mathrm{OD}_R/\mathrm{OD} n^2/{n_R}^2$$

where Q is the QY, I represents the measured integrated emission intensity (emission wavelength of 360 nm), n is the refractive index, and OD is the optical density measured on a UV−vis spectrophotometer, which was limited to less than 0.1. The subscript R stands for the reference fluorophore of known QY.[33] Herein, we chose quinine sulfate dissolved in 0.1 M H_2SO_4 as a reference, whose QY was 0.546 (Q_R = 0.546), and the N-CDs were dissolved in distilled water.

2.6. Mass Extinction Coefficient Measurement. The mass extinction coefficient of CDs is the value at the first absorption peak position. It can be calculated using Lambert−Beer's law.

$$A = \varepsilon CL$$

A is the absorbance at the position of the first excitation absorption peak of C-60. C is the mass concentration (g/L) of C-60. L is the path length (cm) of the radiation beam used for recording the absorption spectrum. In our experiments, L was fixed at 1 cm. ε is the mass extinction coefficient of C-60 (L g^{-1} cm^{-1}). The concentration of C-60 aqueous solution was 0.01 mg mL^{-1}, with A = 0.0702.

2.7. Cytotoxicity Experiment. Human embryonic kidney cell line (AD-293) cells (10^4 cells/150 μL) were first cultured in an incubator containing Dulbecco's modified Eagle's medium (DMEM) for 24 h (37 °C and 5% CO_2) in a 96-well plate. Then, the culture medium was replaced with 100 μL of DMEM containing the N-CDs of different concentrations (0, 50, 100, 200, 400, 800, 1200, and 2000 μg/mL) and incubated for another 24 h. Afterward, 20 μL of 5 mg/mL 3-(4,5-

dx.doi.org/10.1021/la503969z | Langmuir 2014, 30, 13542−13548

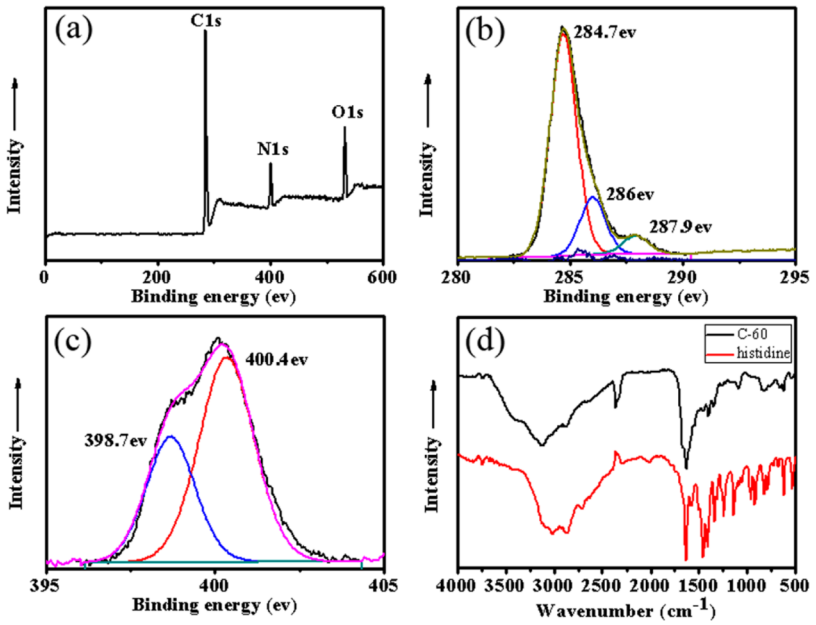

Figure 2. (a) XPS spectra of C-60, (b and c) high-resolution spectra of (b) C_{1s} and (c) N_{1s}, and (d) FTIR spectra of C-60 and histidine.

dimethylthiazol-2-yl)-2,5-diphenyltetrazolium bromide (MTT) solution was added to every cell well, and the cells were further incubated for 4 and 24 h. Then, the culture medium was removed by MTT, followed by the addition of 150 μL of dimethyl sulfoxide (DMSO). The mixture was shaken for 5 min at room temperature. The optical density (OD) of the mixture was measured at 490 nm. The cell viability was estimated using the following equation:

$$\text{cell viability (\%)} = (\text{OD}_{\text{treated}}/\text{OD}_{\text{control}}) \times 100\%$$

where $\text{OD}_{\text{control}}$ was obtained in the absence of N-CDs, and $\text{OD}_{\text{treated}}$ was obtained in the presence of N-CDs.

2.8. Cellular Imaging. The cells were cultured in a DMEM-supplemented solution containing 10% fetal bovine serum and 1% penicillin/streptomycin. Dulbecco's phosphate buffer saline (DPBS) was used to prepare the N-CD solution with a concentration of 1.0 mg/mL and ultrasonicated for 10 min. An aliquot (typically 0.1 mL) of the suspension was added to the well of a chamber slide and incubated at 37 °C in a 5% CO_2 incubator for 20 h. The excess N-CDs were removed by washing with warm DPBS 3 times, and then, the cells were fixed on the slide for analysis by a fluorescence microscope. The bioimaging photographs were captured with Olympus BX 51 with an excitation wavelength of 365 nm.

3. RESULTS AND DISCUSSION

3.1. Synthesis and Characterization of the N-CDs. Histidine, a nitrogen-rich amino acid, was used as a sole carbon source to synthesize the N-CDs through a one-pot microwave-assisted hydrothermal method without involvement of acid, alkali, salt, or organic solvent. Such an environmentally friendly approach leads to the synthesis of N-CDs with functional groups through the selection of carbon sources. The colorless and transparent histidine solution is non-emissive in the visible region under UV light. After the microwave-assisted hydrothermal reaction, the solution changed from colorless to dark brown, where the as-synthesized N-CDs were freely dispersed in the aqueous solution with a transparent appearance without further ultrasonic dispersion. Herein, different reaction times were investigated, i.e., 10, 30, and 60 min, which led to products designated as C-10, C-30, and C-60 accordingly, with similar graphite structures as seen in Figure S1 of the Supporting Information (when the reaction procedure was longer than 60 min, the solution had no fluorescence). Because C-60 has the best photoluminescence property (highest QY that could be seen in Table 1 of the Supporting Information) and narrowest size distribution among them, it will be discussed in detail in the following sections.

3.1.1. Synthesis and Formation Mechanism of N-CDs. As shown in Figure 1, C-60 was well-dispersed, with an average size of 2.7 nm and a narrow size distribution. The TEM images of C-60 (Figure 1a) indicate that C-60 was graphitic carbon with apparent lattice fringes. The well-resolved TEM images indicate that C-60 had an interplanar spacing of 0.32 nm (inset of Figure 1a), which is consistent with the (002) lattice planes of graphitic carbon. This result agrees with the XRD pattern of C-60 (Figure 1c) centered at 24°, which is attributed to the diffraction of the (002) lattice plane.[34] Two broad peaks at around 1355 and 1575 cm^{-1} could be seen from the Raman spectrum of C-60 (Figure 1d), which are in correspondence with the D band (sp^3-hybridized) and G band (sp^2-hybridized), respectively. The D band is attributed to the vibrations of carbon atoms with dangling bonds in the termination plane of disordered graphite or glassy carbon, whereas the G band is related to the vibration of sp^2-hybridized carbon atoms in a two-dimensional hexagonal lattice.[35] The relative intensity of the disordered D band and crystalline G band (I_D/I_G) in regard to C-60 is around 0.7, suggesting that they share structural similarities with graphite.

The structure and components of C-60 were identified by XPS and FTIR experiments. As illustrated in Figure 2a, the XPS spectra show three strong peaks at 532.0, 401.1, and 285.1 eV, revealing the presence of O 1s, N 1s, and C 1s, respectively. The high-resolution spectrum of C 1s shows three main peaks (Figure 2b). The binding energy peak at 284.7 eV confirms the graphitic structure (sp^2 C−C) of C-60. The peaks at about 286.0 and 287.9 eV indicate the presence of C−O and C−N and of C═O, respectively. The N 1s spectrum (Figure 2c) demonstrates the doping of both pyridinic (398.7 eV) and pyrrolic (400.4 eV) N atoms.[21] The carboxylic and amide groups were well-preserved on the surface of C-60 (a high yield of 86.2%) after the carbonization process, which can be proven

dx.doi.org/10.1021/la503969z | Langmuir 2014, 30, 13542−13548

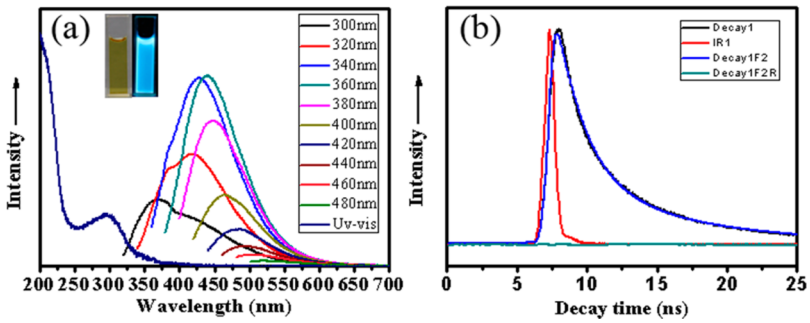

Figure 3. (a) UV absorption and PL emission spectra of C-60 under different excitation wavelengths with 20 nm in increments from 300 to 480 nm, (inset) optical images under (left) daylight and (right) UV light, and (b) photoluminescence lifetime of C-60 and the parameter generated by the exponential fitting (λ_{ex} = 360 nm, and λ_{em} = 439 nm). The concentration of C-60 is 0.01 mg mL^{-1}.

by the FTIR spectra (Figure 2d). The presence of carboxylic groups can be demonstrated by the stretching vibrations of C═O (1550 cm^{-1}) and the vibration of both C−O (1088 cm^{-1}) and −OH (3124 cm^{-1}), whereas the existence of amide groups can be proven by the stretching vibrations of amide I, amide II, N−H, and amide III centered at 1628 and 1458 cm^{-1} and the broad band centered at 2877 cm^{-1}, which was attributed to $-NH_2$ and $-NH_3^+$.[32]

Different reaction time durations were performed to further elucidate the formation mechanism of the CDs. HRTEM images of C-10 and C-30 were shown in Figure S1 of the Supporting Information, which indicated almost identical morphology of the obvious lattice fringes as that of C-60. The average size of C-10 and C-30 was 4.5 and 4.0 nm, respectively (the average size of C-60 is 2.7 nm). The average size decreases with reaction time duration. Elemental analysis (see Table 1 of the Supporting Information) indicates an increase in the quantity of carbon with a prolonged reaction procedure, suggesting that N-CDs underwent further carbonization. The photographs of C-10, C-30, and C-60 powders also demonstrate a higher carbonization degree because the color changed from yellow to brown and then black (see Figure S2 of the Supporting Information). A possible formation mechanism of the CDs is proposed as follows. Because of the high energy supplied by the microwave-assisted hydrothermal treatment, the temperature (200 °C) and pressure inside the reaction vessel enabled histidine to experience dehydration, condensation, polymerization, and carbonization processes via reaction between the amino and carboxyl groups of histidine.[28] As a result, N-CDs were produced via such reactions. With reaction time duration increased, the carbonization degree of the N-CDs increased, which tuned the resultant product into a darker color.

3.1.2. Photoluminescence Property of N-CDs and Its Mechanism. C-60 in an aqueous solution exhibited a strong absorption peak centered at 294 nm (Figure 3a), similar to that of previously reported CDs produced by the microwave-assisted method.[36] This characteristic absorption peak at 294 nm could be ascribed to the $\pi-\pi^*$ electron transition of the conjugated C═C band and the n−π^* electron transition of the C═O band.[37] In the fluorescence spectra, the optimal excitation and emission wavelengths of C-60 centered at 360 and 439 nm, showing a blue color under a hand-held UV lamp (Figure 3a). The inset in Figure 3a shows the optical images of the CDs under illumination of sunlight and UV light (365 nm, center). C-60 exhibits a bright blue photoluminescence, which is strong enough to be easily recognized by the naked eye. Its excitation-dependent PL behavior is similar to that of fluorescent carbon materials.[17,19,20] It is believed that this phenomenon could be attributed to emissive traps, electronic conjungate structures, and free zigzag sites of the CDs. Using quinine sulfate as a reference, the PL QY of C-10, C-30, and C-60 was 1.4, 2.5, and 8.9%, respectively (see Table 2 of the Supporting Information). As shown in the TEM images of the N-CDs (Figure 1 and Figure S1 of the Supporting Information), all of the N-CDs have a graphitic structure; therefore, the strong fluorescence exhibited by the CDs may be mainly attributed to the quantum confinement of the passivated surface energy traps. The isolated sp^2 carbon atoms dispersed within a sp^3 carbon atom matrix can act as PL centers, which depend upon the π states of sp^2 domains. In particular, the photogeneration of electron−hole pairs can lead to the radiative recombination of the trap carriers localized within sp^2 sites surrounded by sp^3 defects, which could result in the PL mechanism of amorphous/disordered graphites containing a mixture of sp^2 and sp^3 carbons. This mechanism can remain effective in the presence of heteroatoms.[38] With a longer reaction procedure, the N-CDs were better carbonized with better surface states and had a higher QY. Therefore, C-60 has the highest QY among the three of them. The excitation-independent PL behavior of the CDs also suggests that the strong fluorescence of the N-CDs depends upon surface states rather than morphology.

Generally, fluorescence lifetime measurement can be conducted to help understand the fluorescence mechanism of CDs, which mainly concerns the CDs and their environment. In this study, the fluorescence lifetime of C-60 was assessed by time-resolved photoluminescence measurements. As shown in Figure 3b, the decay trace was fitted using bi-exponential functions $Y(t)$ based on a nonlinear least-squares analysis according to the following equation:

$$Y(t) = A_1 \exp(-t/s_1) + A_2 \exp(-t/s_2)$$

where A_1 and A_2 are the fractional contributions of time-resolved decay lifetime of s_1 and s_2. The bi-exponential behavior of the lifetime suggests that two different emissive sites are present. This implies that the fluorescence state is due to the graphite center (or conjugated structures) and surface traps.[39] Furthermore, we calculated the average lifetime ($S_{average}$) of C-60 using $S_{average} = A_1 \exp(-t/s_1) + A_2 \exp(-t/s_2)$ as 5.71 ns, which is comparable to other reported values.[9] Such excitation-dependent PL behavior makes the as-prepared CDs appropriate candidates for extensive applications, such as bioimaging, biolabeling, and development of optoelectronic devices. The

dx.doi.org/10.1021/la503969z | Langmuir 2014, 30, 13542−13548

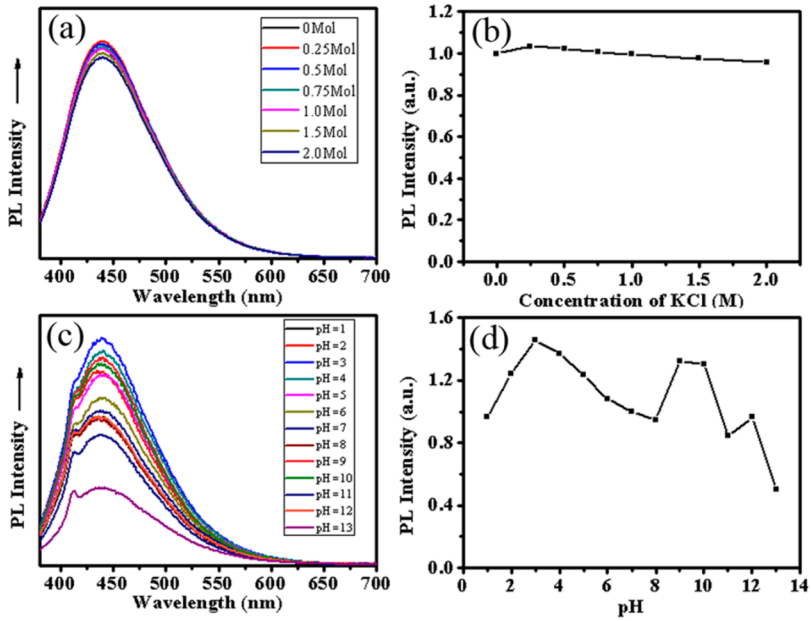

Figure 4. (a) PL spectra of C-60 in KCl solutions of different concentrations, (b) PL spectra of C-60 in KCl solutions of different concentrations after normalization, (c) PL spectra of C-60 in different pH aqueous solutions ranging from 1 to 13, and (d) PL spectra of C-60 with different pH values after normalization. The concentration of C-60 is 0.01 mg mL^{-1}.

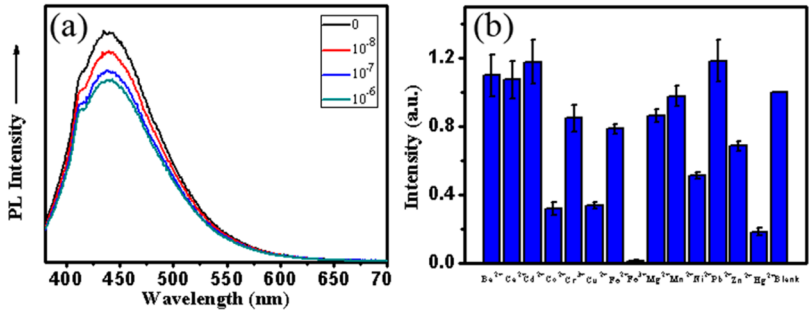

Figure 5. (a) PL spectra of C-60 in aqueous solution with different Fe^{3+} concentrations (0, 10^{-8}, 10^{-7}, and 10^{-6} M) and (b) PL spectra of C-60 aqueous solution in the presence of different metal ions (the concentration of different metal ions is 10^{-3} M, and the concentration of C-60 is 0.01 mg mL^{-1}).

extinction coefficient of CDs could be essential for convenient and accurate measurements of the concentrations of CDs. The mass extinction coefficient of C-60 was defined as 7.02 L g^{-1} cm^{-1} according to Lambert−Beer's law.

Even without any further surface passivation, the as-obtained N-CDs possess excellent solubility (more than 24 mg mL^{-1}) in water without any further surface passivation, which may originate from the −OH, $-NH_3^+$, and −COOH groups on the surface of the N-CDs. The PL property of C-60 at different ionic strengths was monitored in KCl solution with varying concentrations from 0 to 2.0 M. As shown in Figure 4a, there were barely changes in either the PL intensities or the peak characteristics, which is of benefit for the use of C-60 in KCl solutions. The stability of the CDs in salty conditions ensures their applications in sophisticated and harsh conditions. Another interesting phenomenon is the pH-dependent PL behavior, in which PL intensities increased in solutions with pH higher or lower than 7. pH of ca. 5 and C-60 exhibited the highest PL intensity (panels c and d of Figure 4), except when the pH was higher than 12, which is different from previously reported N-CDs. The −OH, $-NH_3^+$, and −COOH groups on the surface of the N-CDs may contribute to this interesting phenomenon. The photoluminescence of N-CDs is strong and stable over a wide range of pH values and ion strength. An obvious photobleaching phenomenon was observed after continuous exposure under UV excitation for 5 h using a hand-held UV lamp (see Figure S3 of the Supporting Information), which indicated the unstable surface states of the N-CDs under long-time UV irradiation.

3.2. Metal Ion Sensing Capability of N-CDs. CDs can serve as a sensing candidate because the oxygen-containing groups on the surface of CDs can coordinate with transition metal ions. Iron is an indispensable element in life. A high concentration of Fe^{3+} is toxic to living organisms, causing diseases, such as Parkinson's, Alzheimer's, etc. Therefore, the detection of Fe^{3+} is of vital importance. C-60 contains ample functional groups, such as −OH, $-NH_3^+$, and −COOH, and the PhOH could generate complexes with Fe^{3+} because of the synergistic effect, making it possible to detect Fe^{3+}. In the present study, the PL spectra of C-60 aqueous solutions with different amounts of the Fe^{3+} ion were collected to prove the viability to detect the Fe^{3+} ion. Fe^{3+} can quench the fluorescence of C-60 effectively with a limit of detection (LOD) of 10^{-8} M (10 nM) (Figure 5a). The Fe−(N-CD)

dx.doi.org/10.1021/la503969z | Langmuir 2014, 30, 13542−13548

complex could accelerate the excition transfer and regulate the charge recombination, resulting in an obvious fluorescence quenching.[40] In addition to hypersensitivity to Fe^{3+}, the selectivity of our N-CDs toward different metal ions has also been taken into account. Figure 5b exhibits the PL spectra of C-60 in the environment of various metal ions, such as Fe^{3+}, Ba^{2+}, Fe^{2+}, Pb^{2+}, and Hg^{2+} (each of the concentrations is 10^{-3} M). Various influences on the PL intensity were observed in the existence of different metal ions. In comparison to other metal ions, Fe^{3+} shows the most obvious quenching effect on the PL intensity. The hypersensitivity as well as hyperselectivity to Fe^{3+} makes the N-CDs a promising fluorescent sensing agent for highly efficient detection of Fe^{3+}.

3.3. Toxicity of the N-CDs and Its Bioimaging Application. Fluorescent CDs have drawn much attention especially for their application as optical imaging agents because of their excellent biocompatibility, low toxicity, and chemical stability. In the present research, C-60 (QY of 8.9%) was used as an optical imaging agent to label the AD-293 (human embryonic kidney) cells (the QY of C-60 was not very high but is adequate for bioimaging applications[41]). Low toxicity is a key consideration in bioimaging. The MTT assay method was used to assess the cytotoxicity of C-60. AD-293 cells were cultured in the medium with different concentrations of C-60 for 24 h. The results are shown in Figure 6a. The viability of AD-293 cells

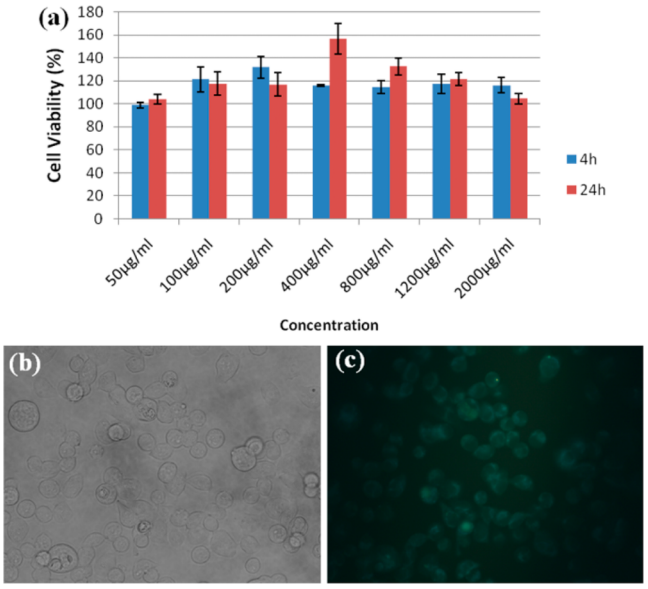

Figure 6. (a) Cellular toxicity of C-60 on AD-293 cell viability, (b) cellular image on a bright field, and (c) cellular image on 365 nm excitation.

was almost 100%, even when the concentration of C-60 was 2000 μg/mL after 24 h. Because there was a sort of residual histidine in C-60, which provided nutrition for AD-293 cells, the viability of most of the AD-293 cells was more than 100%, which verified the nontoxicity of C-60. AD-293 cells were cultured in the medium containing 1 mg mL^{-1} C-60 for 20 h and observed under a fluorescence microscope to prove the viability of N-CDs as an ideal bioimaging agent. In Figure 6b, the AD-293 cells treated with C-60 showed bright green color under 365 nm excitation. Interestingly, strong PL was displayed in the cell nucleus as well as in the cytoplasmic area, suggesting the capacity of as-prepared CDs for transporting into the nucleus of AD-293 cells. This nuclear-staining phenomenon is hardly seen in most of the CDs prepared previously. The N-CDs can serve as a promising candidate for *in vivo* imaging and biosensors because of their low toxicity and good biocompatibility. The N-CDs may also be further functionalized by gene or anticancer drugs into the nucleus of cells to realize targeted recognition and therapy.

4. CONCLUSION

N-CDs were prepared through a one-pot microwave-assisted hydrothermal method using histidine as a sole carbon source without additives (acid, alkali, or salt). The N-CDs had a narrow size distribution of 2−5 nm and obvious lattice fringes. Under high temperature and pressure in the reaction vessel, histidine experienced dehydration, condensation, polymerization, and carbonization processes to form the final N-CDs. The as-prepared N-CDs had well-defined surface chemistry and excellent photoluminescence properties. They also had a high yield and good water solubility and are suitable for use in different pH values and KCl aqueous solutions. They were used as a fluorescent probe to detect Fe^{3+} with a detection limit of 10 nM, owing to the presence of −OH groups on the surface. They also possessed low toxicity and perfect biocompatibility and were used as an optical imaging agent to label AD-293 cells. The low toxic CDs can be widely used for optical imaging in both *in vitro* and *in vivo*.

■ ASSOCIATED CONTENT

Supporting Information

TEM images and size distribution of synthesized C-10 and C-30 (Figure S1), photograph and QY of the CDs of different reaction procedures (Figure S2 and Tables 1 and 2), and PL properties of C-60 after UV exposure (Figure S3). This material is available free of charge via the Internet at http://pubs.acs.org.

■ AUTHOR INFORMATION

Corresponding Authors

*C.L.: E-mail: cglee@jlu.edu.cn.

*Z.S.: Telephone/Fax: +86-431-85168662. E-mail: zshi@mail.jlu.edu.cn.

Notes

The authors declare no competing financial interest.

■ ACKNOWLEDGMENTS

This work was supported by the Foundation of the Natural Science Foundation of China (21371069 and 21301068), the Specialized Research Fund for the Doctoral Program of Higher Education (20110061110015), the National High Technology Research and Development Program (863 Program) of China (2013AA031702), and the Special Program of China Postdoctoral Science Foundation (2012T50288).

■ REFERENCES

(1) Michalet, X.; Pinaud, F. F.; Bentolila, L. A.; Tsay, J. M.; Doose, S.; Li, J.; Sundareasan, G.; Wu, A.; Gambhir, S. S.; Wesiss, S. Quantum dots for live cells, in vivo imaging, and diagnostics. *Science* **2005**, *307*, 538−581.

(2) Gao, X.; Cui, Y.; Levenson, R. M.; Chung, L. W. K.; Nie, S. In vivo cancer targeting and imaging with semiconductor quantum dots. *Nat. Biotechnol.* **2004**, *22*, 969−1044.

(3) Medintz, I. L.; Uyeda, H. T.; Goldman, E. R.; Mattoussi, H. Quantum dot bioconjugates for imaging, labeling and sensing. *Nat. Mater.* **2005**, *4*, 435−480.

(4) Su, Y.; He, Y.; Lu, H.; Sai, L.; Li, Q.; Li, W.; Wang, L.; Shen, P.; Huang, Q.; Fan, C. The cytotoxicity of cadmium based, aqueous phase-synthesized, quantum dots and its modulation by surface coating. *Biomaterials* **2009**, *30*, 19−25.
(5) Reiss, P.; Protière, M.; Li, L. Core/shell semiconductor nanocrystals. *Small* **2009**, *5* (2), 154−221.
(6) Kang, Z.; Liu, Y.; Tsang, C.; Ma, D.; Fan, X.; Wong, N.; Lee, S. Water-soluble silicon quantum dots with wavelength-tunable photoluminescence. *Adv. Mater.* **2009**, *21* (6), 661−664.
(7) Chan, W.; Nie, S. Quantum dot bioconjugates for ultrasensitive nonisotopic detection. *Science* **1998**, *281*, 2016−2025.
(8) Hardman, R. A. Toxicologic review of quantum dots: Toxicity depends on physicochemical and environmental factors. *Environ. Health Perspect.* **2006**, *114* (2), 165−236.
(9) Baker, S. N.; Baker, A. J. Luminescent carbon nanodots: emergent nanolights. *Angew. Chem., Int. Ed.* **2010**, *49* (38), 6726−6769.
(10) Li, H.; Kang, Z.; Liu, Y.; Lee, S. Carbon nanodots: Synthesis, properties and applications. *J. Mater. Chem.* **2012**, *22* (46), 24230−24282.
(11) Cao, L.; Meziani, M. J.; Sahu, S.; Sun, Y. Photoluminescence properties of graphene versus other carbon nanomaterials. *Acc. Chem. Res.* **2013**, *46* (1), 171−180.
(12) Ding, C.; Zhu, A.; Tian, Y. Functional surface engineering of C-dots for fluorescent biosensing and in vivo bioimaging. *Acc. Chem. Res.* **2014**, *47* (1), 20−30.
(13) Sun, Y.; Zhou, B.; Lin, Y.; Wang, W.; Fernando, K. A. S.; Pathak, P.; Meziani, M. J.; Harruff, B. A.; Wang, X.; Wang, H.; Luo, P.; Yang, H.; Kose, M. E.; Chen, B. L.; Veca, L. M.; Xie, S. Quantum-sized carbon dots for bright and colorful photoluminescence. *J. Am. Chem. Soc.* **2006**, *128* (24), 7756−7762.
(14) Wang, X.; Cao, L.; Yang, S.; Lu, F.; Meziani, M. J.; Tian, L.; Sun, K.; Bloodgood, M. A.; Sun, Y. Bandgap-like strong fluorescence in functionalized carbon nanoparticles. *Angew. Chem., Int. Ed.* **2010**, *49* (31), 5310−5314.
(15) Hu, S.; Niu, K.; Sun, J.; Yang, J.; Zhao, N.; Du, X. One-step synthesis of fluorescent carbon nanoparticles by laser irradiation. *J. Mater. Chem.* **2009**, *19* (4), 484−491.
(16) Xu, X.; Ray, R.; Gu, Y.; Ploehn, H. J.; Gearheart, L.; Raker, K.; Scrivens, W. A. Electrophoretic analysis and purification of fluorescent single-walled carbon nanotube fragments. *J. Am. Chem. Soc.* **2004**, *126* (40), 12736−12737.
(17) Bao, L.; Zhang, Z.; Tian, Z.; Zhang, L.; Liu, C.; Lin, Y.; Qi, B.; Pang, D. Electrochemical tuning of luminescent carbon nanodots: from preparation to luminescence mechanism. *Adv. Mater.* **2011**, *23* (48), 5801−5806.
(18) Yu, H.; Zhao, Y.; Zhou, C.; Shang, L.; Peng, Y.; Cao, Y.; Wu, L.; Tung, C.; Zhang, T. Carbon quantum dots/TiO_2 composites for efficient photocatalytic hydrogen evolution. *J. Mater. Chem. A* **2014**, *10* (2), 3344−3351.
(19) Li, W.; Zhang, Z.; Kong, B.; Feng, S.; Wang, J.; Wang, L.; Yang, J.; Zhang, F.; Wu, P.; Zhao, D. Simple and green synthesis of nitrogen-doped photoluminescent carbonaceous nanospheres for bioimaging. *Angew. Chem., Int. Ed.* **2013**, *52* (31), 8151−8155.
(20) Hsu, P.; Chang, H. Synthesis of high-quality carbon nanodots from hydrophilic compounds: Role of functional groups. *Chem. Commun.* **2012**, *48* (33), 3984−3986.
(21) Dong, Y.; Pang, H.; Yang, H.; Guo, C.; Shao, J.; Chi, Y.; Li, C.; Yu, T. Carbon-based dots co-doped with nitrogen and sulfur for high quantum yield and excitation-independent emission. *Angew. Chem., Int. Ed.* **2013**, *52* (30), 7800−7803.
(22) Wang, F.; Xie, Z.; Zhang, H.; Liu, C.; Zhang, Y. Highly luminescent organosilane-functionalized carbon dots. *Adv. Funct. Mater.* **2011**, *21* (6), 1027−1031.
(23) Tang, L.; Ji, R.; Cao, X.; Lin, J.; Jiang, H.; Li, X.; Teng, K. S.; Luk, C. M.; Zeng, S.; Hao, J.; Lau, S. P. Deep ultraviolet photoluminescence of water-soluble self-passivated graphene quantum dots. *ACS Nano* **2012**, *6* (6), 5102−5110.
(24) Liu, R.; Wu, D.; Liu, S.; Koynov, K.; Knoll, W.; Li, Q. An aqueous route to multicolor photoluminescent carbon dots using silica spheres as carriers. *Angew. Chem., Int. Ed.* **2009**, *48* (25), 4598−4601.
(25) Li, H.; He, X.; Liu, Y.; Huang, H.; Lian, S.; Lee, S.; Kang, Z. One-step ultrasonic synthesis of water-soluble carbon nanoparticles with excellent photoluminescent properties. *Carbon* **2011**, *49* (2), 605−609.
(26) Sevilla, M.; Fuertes, A. B. Chemical and structural properties of carbonaceous products obtained by hydrothermal carbonization of saccharides. *Chem.—Eur. J.* **2009**, *15* (16), 4195−4203.
(27) Liu, C.; Zhang, P.; Tian, F.; Li, W.; Li, F.; Liu, W. One-step synthesis of surface passivated carbon nanodots by microwave assisted pyrolysis for enhanced multicolor photoluminescence and bioimaging. *J. Mater. Chem.* **2011**, *21* (35), 13163−13167.
(28) Zhu, S.; Meng, Q.; Wang, L.; Zhang, J.; Song, Y.; Jin, H.; Sun, H.; Wang, H.; Yang, B. Highly photoluminescent carbondots for multicolor patterning, sensors, and bioimaging. *Angew. Chem., Int. Ed.* **2013**, *125* (14), 4045−40459.
(29) Zhu, C.; Zhai, J.; Dong, S. Bifunctional fluorescent carbon nanodots: green synthesis via soy milk and application as metal-free electrocatalysts for oxygen reduction. *Chem. Commun.* **2012**, *48* (75), 9367−9369.
(30) Lu, W.; Qin, X.; Liu, S.; Chang, G.; Zhang, Y.; Luo, Y.; Asiri, A. M.; Al-Youbi, A. O.; Sun, X. Economical, green synthesis of fluorescent carbon nanoparticles and their use as probes for sensitive and selective detection of mercury(II) ions. *Anal. Chem.* **2012**, *84* (12), 5351−5357.
(31) Huang, H.; Lv, J.; Zhou, D.; Bao, N.; Xu, Y.; Wang, A.; Feng, J. One-pot green synthesis of nitrogen-doped carbon nanoparticles as fluorescent probes for mercury ions. *RSC Adv.* **2013**, *3* (44), 21691−21696.
(32) Jiang, J.; He, Y.; Li, S.; Cui, H. Amino acids as the source for producing carbon nanodots: Microwave assisted one-step synthesis, intrinsic photoluminescence property and intense chemiluminescence enhancement. *Chem. Commun.* **2012**, *48* (77), 9634−9636.
(33) Murase, N.; Li, C. Consistent determination of photoluminescence quantum efficiency for phosphors in the form of solution, plate, thin film, and powder. *J. Lumin.* **2008**, *128* (12), 1896−1903.
(34) Peng, H.; Travas-Sejdic, J. Simple aqueous solution route to luminescent carbogenic dots from carbohydrates. *Chem. Mater.* **2009**, *21* (23), 5563−5565.
(35) Qu, S.; Wang, X.; Lu, Q.; Liu, X.; Wang, L. A biocompatible fluorescent ink based on water-soluble luminescent carbon nanodots. *Angew. Chem., Int. Ed.* **2012**, *51* (49), 12215−12218.
(36) Wang, Q.; Zheng, H.; Long, Y.; Zhang, L.; Gao, M.; Bai, W. Microwave−hydrothermal synthesis of fluorescent carbon dots from graphite oxide. *Carbon* **2011**, *49* (9), 3134−3140.
(37) Jia, X.; Li, J.; Wang, E. One-pot green synthesis of optically pH-sensitive carbon dots with upconversion luminescence. *Nanoscale* **2012**, *18* (4), 5572−5575.
(38) Krysmann, M. J.; Kelarakis, A.; Dallas, P.; Giannelis, E. P. Formation mechanism of carbogenic nanoparticles with dual photoluminescence emission. *J. Am. Chem. Soc.* **2012**, *134* (2), 747−750.
(39) Peng, J.; Gao, W.; Gupta, B.K.; Liu, Z.; Romero-Aburto, R.; Ge, L.; Song, L.; Alemany, L. B.; Zhan, X.; Gao, G.; Vithayathil, S. A.; Kaipparettu, B. A.; Marti, A. A.; Hayashi, T.; Zhu, J.; Ajayan, P. M. Graphene quantum dots derived from carbon fibers. *Nano Lett.* **2012**, *12* (2), 844−848.
(40) Zhang, Y.; Wang, L.; Zhang, H.; Liu, Y.; Wang, H.; Kang, Z.; Li, S. Graphitic carbon quantom dots as a fluorescent sensing platform for highly efficient detection of Fe^{3+} ions. *RSC Adv.* **2013**, *3* (11), 3733−3738.
(41) Zhu, S.; Zhang, J.; Wang, L.; Song, Y.; Zhang, G.; Wang, H.; Yang, B. A general route to make non-conjugated linear polymers luminescent. *Chem. Commun.* **2012**, *88* (48), 10889−10891.